Applied Thermal Engineering 113 (2017) 1170–1177

Contents lists available at ScienceDirect

Applied Thermal Engineering

journal homepage: www.elsevier.com/locate/apthermeng

Research Paper

Using artificial neural network models and particle swarm optimization for manner prediction of a photovoltaic thermal nanofluid based collector

Hadi Kalani [a], Mohammad Sardarabadi [b,*], Mohammad Passandideh-Fard [b]

[a] Center of Excellence on Soft Computing and Intelligent Information Processing (SCIIP), Mechanical Engineering Department, Ferdowsi University of Mashhad, Mashhad, Iran
[b] Micro/Nanofluidic & MEMS Laboratory (MNL), Mechanical Engineering Department, Ferdowsi University of Mashhad, Mashhad, Iran

HIGHLIGHTS

- In this study, different neural networks are used for modeling PVT/N systems.
- Experiments are performed on ZnO/water nanofluid (0.2 wt%).
- Particle Swarm Optimization (PSO) is used to find optimum structure of each model.
- Results of three models are compared and validated with the experiments.
- Neural networks can be well used in modeling nanofluid based solar systems.

ARTICLE INFO

Article history:
Received 4 February 2016
Revised 3 September 2016
Accepted 13 November 2016
Available online 15 November 2016

Keywords:
Photovoltaic thermal system
Nanofluid
Particle Swarm Optimization (PSO)
Neural network

ABSTRACT

The present study introduces a new approach to model a photovoltaic thermal nanofluid based collector system (PVT/N). Two artificial neural networks of radial-basis function artificial neural network (RBFANN) and multi-layer perception artificial neural network (MLPANN), as well as adaptive neuro fuzzy inference system (ANFIS) model are used to identify a complex non-linear relationship between input and output parameters of the PVT/N system. Fluid outlet temperature of the collector and the electrical efficiency of the photovoltaic unit (PV) are selected as two essential output parameters of the PVT/N system. In each model, the optimized structure is obtained through a Particle Swarm Optimization (PSO) technique. Zinc-oxide/water nanofluid is considered as the working fluid of the PVT/N setup. Experiments are repeated in ten days with thirteen data points in each day such that different environmental conditions are included in the measurements. Results of the three above-mentioned models are compared and validated with those of the measurements. All three models were found to be reasonably capable of estimating the performance of the PVT/N system. Moreover, the analysis of variance (ANOVA) results indicated that the ANFIS and RBFANN were more accurate in predicting the electrical efficiency and fluid outlet temperature, respectively.

1. Introduction

Photovoltaic thermal (PVT) systems consist of a heat recovery mechanism integrated with a conventional photovoltaic module. These systems, by absorbing the extra heat of the photovoltaic cells, in addition to an increase of the electrical efficiency, can produce useful thermal energy that leads to more system performance [1]. The PVT systems have been studied considerably in the literature by all means of analytical solutions [2,3], experimental measurements [1,4,5], and numerical simulations [6,7]. By using a nanofluid as the coolant in the PVT systems, a large portion of primary materials used to fabricate the system can be eliminated based on the scaling of the overall percentage weight of the collector. Employing nanofluids in solar collectors results in more energy savings using a smaller size system with less CO_2 emission.

Recently, artificial neural networks (ANNs) have been significantly employed in different fields by researchers, especially in energy systems [8]. Ability to find the relationship between inputs/outputs and also to have high speed simulations are the known benefits of these networks [9]. Renno et al. [10] applied the ANN models for predicting the solar radiation as input of a

* Corresponding author.
E-mail address: m.sardarabadi@yahoo.com (M. Sardarabadi).

http://dx.doi.org/10.1016/j.applthermaleng.2016.11.105
1359-4311/

concentrating PVT system. They used multi-layer perceptron artificial neural network (MLPANN) for predicting solar global radiation and direct normal solar irradiance. They showed that the ANNs models can estimate daily global radiation and direct normal solar irradiance with a reasonable accuracy. Celik [11] used the generalized regression neural network to forecast the operating current of mono-crystalline photovoltaic modules. He compared the estimated results with those of the analytical model. He concluded that the ANN modeling provides a better prediction of the current than the analytical model. A similar study can be seen in the works of Leva et al. [12], Mellit et al. [13] and Ceylan et al. [14].

The ANN model is not only useful in predicting the electrical performance of the systems, but also it can be employed to predict the thermal performance of the mechanical systems such as heat exchangers [15]. Therefore, using the ANN can be an appropriate methodology to predict the dynamic behavior of a photovoltaic thermal systems under internal and external conditions such as climate changes, the fluid mass flow rate, and the system design. Gunasekar et al. [16] used the ANN for medeling a photovoltaic-thermal evaporator of solar assisted heat pumps. They used experimental results in training the network. Their results indicated that solar intensity and ambient temperature are the most influencing parameters on the energy performance of PVT evaporators.

Many studies showed that the ANNs are capable in simulating and predicting variables in nanofluids, such as thermal conductivity [17–19], viscosity [20,21], density [22] and heat transfer [23,24] in various conditions. As a result, the ANNs can be used in the systems involving nanofluids. These systems have been studied considerably in the literature by all means of analytical solutions, experimental measurements, and numerical simulations.

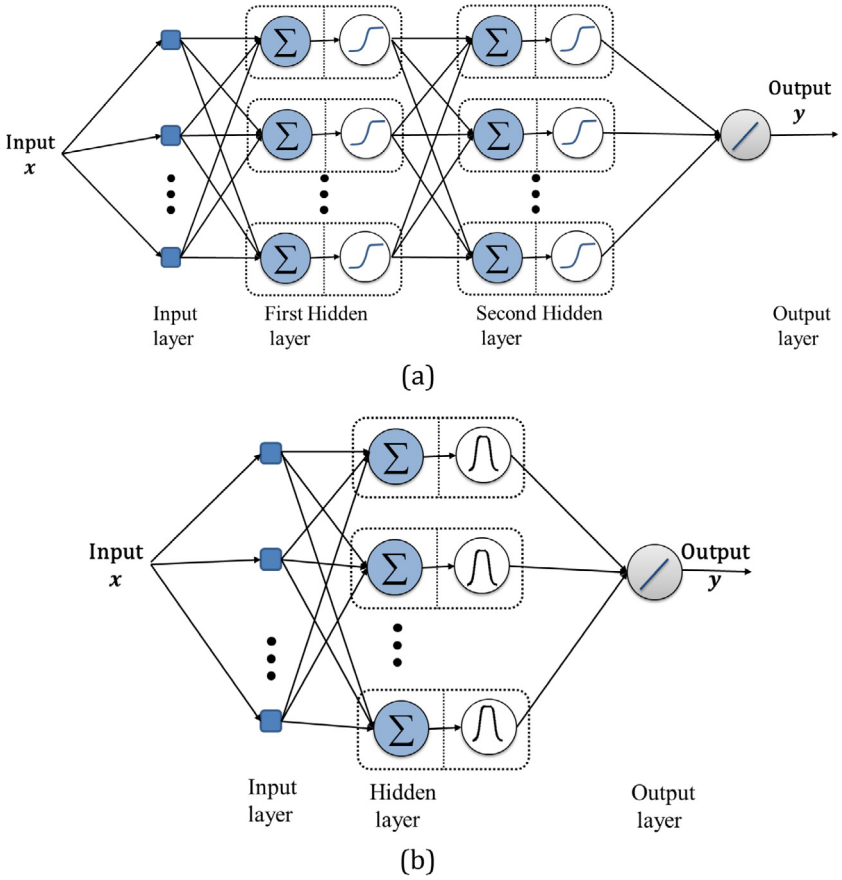

Fig. 1. Structural diagram of the ANN: (a) MLPANN architecture; (b) RBFANN architecture.

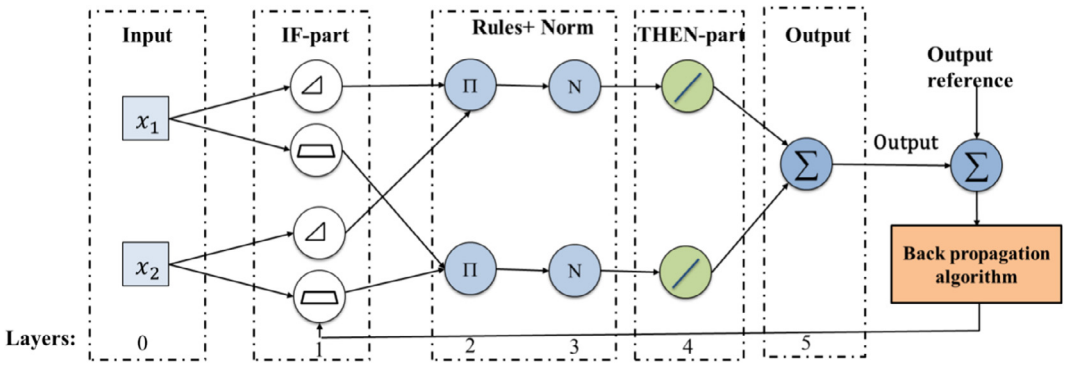

Fig. 2. Structural diagram of the ANFIS.

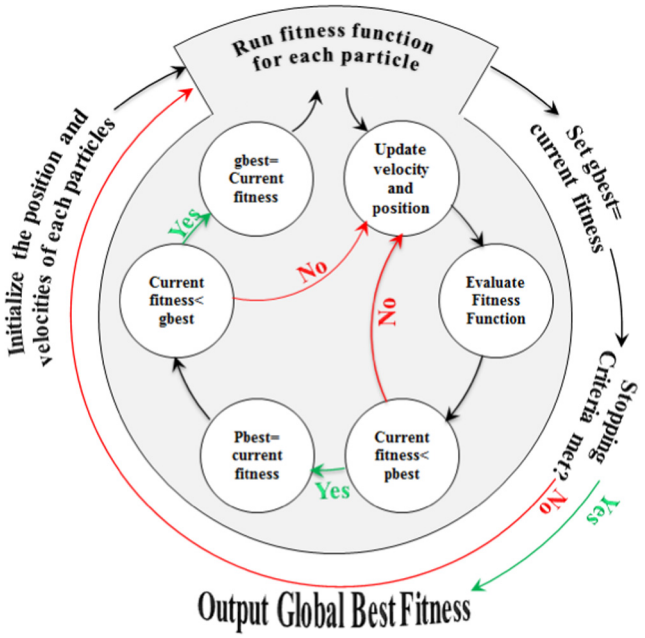

Fig. 3. Flowchart of the PSO method.

Table 1
Optimization parameters in different neural methods.

MLPANN	• number of hidden layers: {1, 2} • number of neuron in each hidden layers: {5, 25} • Activation function in each hidden layers: {logsig and tansig}
RBFANN	• spread of the Gaussian basis function {1, 10} • number of neurons: {5, 20}
ANFIS	• number of Membership function for each inputs {2, 3} • type of input membership functions: {Product of two sigmoidal, Difference between two sigmoidal functions, Gaussian curve, Generalized bell-shaped, Π-shaped, Trapezoidal-shaped, Triangular-shaped}

Although the ANN has been studied in many applications, to the best of authors knowledge, there is few works reported on modeling of the PVT/N systems by these methods. In this study, therefore, three methods of the MLPANN, RBFANN and ANFIS are used to model a PVT/N system. These methods are explained in Section 2. In Section 3, the PSO is used to find the best structure for each method in modeling the PVT/N system. The experimental setup and protocol are explained in Section 4. Finally, the performance of the MLPANN, RBFANN and ANFIS in predicting the output parameters is presented in Section 5.

2. Artificial neural network and ANFIS models

Neural networks are the remarkable methods in pattern classification problems. Radial-basis function artificial neural network (RBFANN) and Multi-Layer Perceptron artificial neural network (MLPANN) are two of the most widely used neural network architecture. These two methods are both known as universal approximates for nonlinear input-output mapping. It should be noted that, the main difference between the MLPANN and RBFANN is that the output of a MLPANN is calculated by linear combinations of the outputs of hidden layer nodes that are obtained by a weighted average of the inputs through a sigmoid function. Although outputs of RBFANN are produced by mapping distances between input vectors and center vectors to output through a nonlinear kernel. Moreover, the MLPANN can have more than one hidden layer, while the RBFANN network has only a single hidden layer. A Levenberg Marquardt (LM) algorithm is used for back-propagation training of the network. A schematic of the MLPANN and RBFANN are shown in Fig. 1a and b, respectively. To enhance the ability of a neural network in learning, a fuzzy logic is employed. The combination of the ANN and fuzzy logic is called the adaptive neuro-fuzzy inference system (ANFIS). In this paper, a hybrid algorithm is used to learn the ANFIS which is a combination of gradient descent and the least-squares method. Fig. 2 shows the structure of the ANFIS with two inputs and one output. In this study, we assume that the MLPANN, RBFANN and ANFIS have three inputs and one output.

3. Choice of structural parameters by PSO

In this work, the PSO is employed to obtain optimized parameters in each method. The PSO has widely been used in the literature for optimization of complicated dynamic systems. Kennedy and Russell [25] proposed this method in 1995. The PSO is appropriated

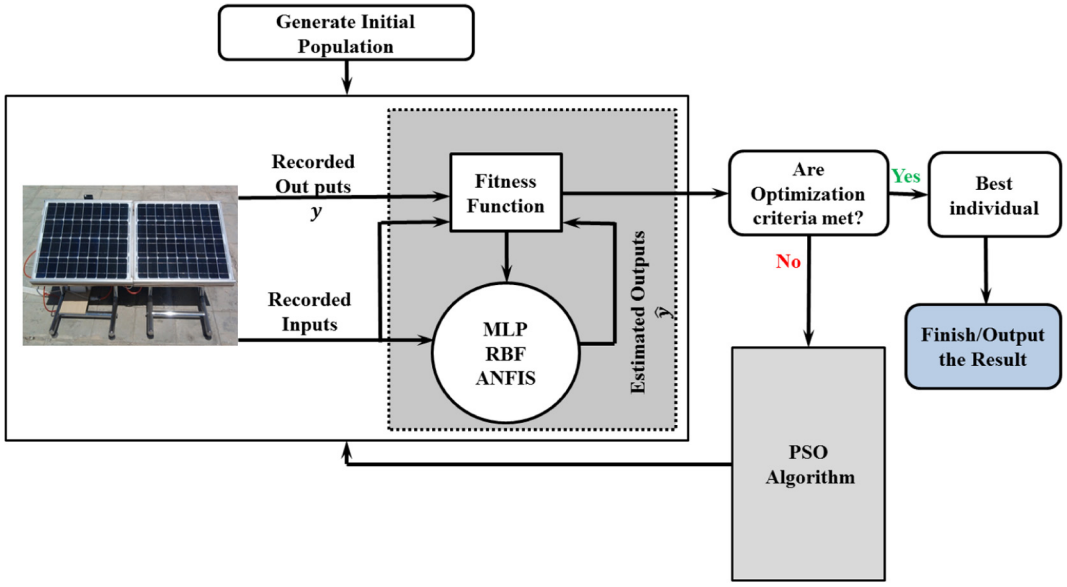

Fig. 4. Block diagram of the proposed technique.

for the derivation of the global optimum. It is also simple and has a high tracing accuracy as well as fast convergence [29]. The PSO is capable of exploring the solution space of a given problem to find the best answers given a particular objective function. This method is inspired by the natural social behavior and movement of insects, birds and fishes [25–28]. In comparison with genetic algorithm where mutation and crossover are used as evolutionary operators, in the PSO a flock of particles is placed in the search space. Each particle updates its travelling speed dynamically based on the flying experiences of itself and its colleagues, meaning each particle improves its position based on (1) its current position, (2) its current velocity, (3) the distance between its current position and the best particle (p-best) and finally the distance between its current position and the global best particle (g-best) [25–29]. Fig. 3 depicts the general schematic of the PSO method. Table 1, shows the parameters that are optimized in the MLPANN, RBFANN and ANFIS. Based on Fig. 4, the role of the PSO is to find the best reference value for the prediction process, while the ANN (MLPANN and RBFANN) and ANFIS search for the best mapping function to predict the targets based on the schematic provided by the PSO. On the other hand, to obtain the best possible results, a fitness function is denoted based on the error of the methods, as follows:

$$F = ||y - \hat{y}|| + \max(y - \hat{y}) + \mathrm{std}(y - \hat{y}) \quad (1)$$

where y and $\hat{y}$ represent the target and output vectors of the training process, respectively. The absolute values of error, the maximum and standard deviation are used in the fitness function, which forces the algorithm to focus on reducing the maximum and minimum error ranges.

The optimized parameters for each method are obtained separately. After the optimized network is found, the evaluation criteria are used to validate the trained model. These criteria are root mean square error (RMSE), variance accounted for (VAF) and mean absolute percentage error (MAPE) that are formulated as given below

$$\mathrm{RSME} = \sqrt{\frac{1}{n}\sum_{i=1}^{n}(y_i - \hat{y}_i)^2} \quad (2)$$

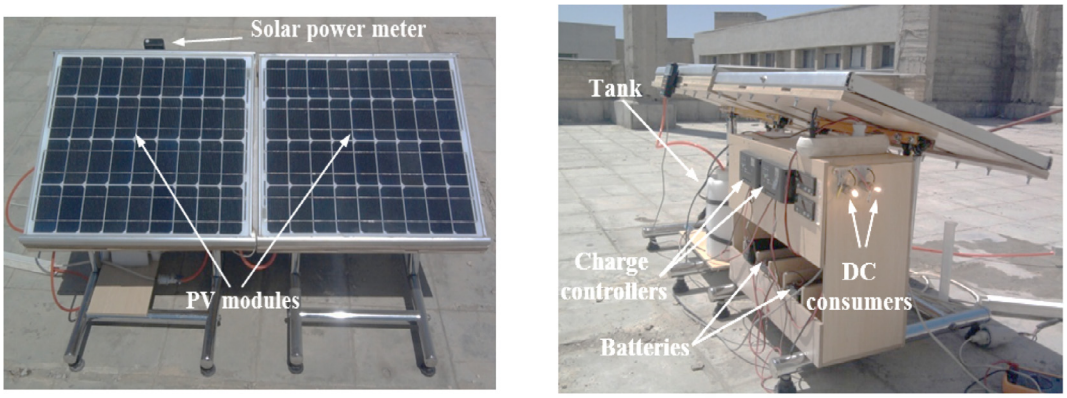

(a) (b)

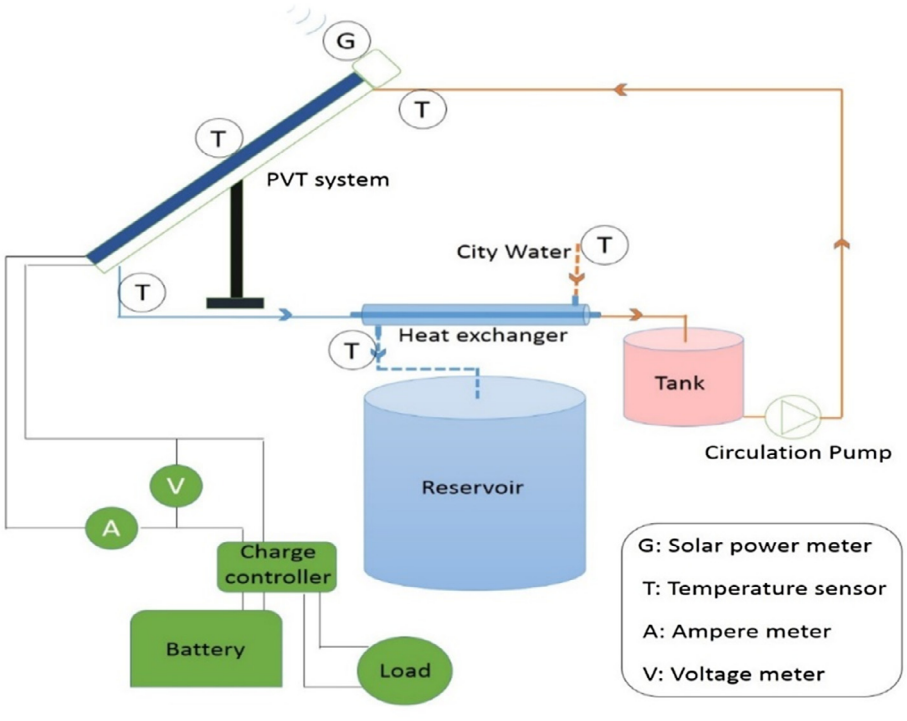

(c)

Fig. 5. Experimental setup installed at the Ferdowsi University of Mashhad (FUM), Mashhad, Iran. (a) Front view, (b) side view and (c) schematic diagram.

$$VAF = \left[1 - \frac{var(y - \hat{y})}{var(y)}\right] \quad (3)$$

$$MAPE = \frac{1}{n}\sum_{i=1}^{n}\left|\frac{y_i - \hat{y}_i}{y_i}\right| \quad (4)$$

where y_i and $\hat{y}_i$ are the measured and the estimated output, respectively, and n is the number of samples.

From the experiments, the proposed system was trained by 130 points (ten sets of the experiments) of the recorded data, while validation was performed with thirteen points (a set of the experiment) of a different experimental condition. Ambient temperature, incident radiation and fluid inlet temperature are used as inputs. On the other hands, fluid outlet temperature and electrical efficiency are set as output parameters of the system.

4. Experimental setup

The experimental setup consisted of 40 W mono crystalline silicon photovoltaic module. As a PVT system the photovoltaic unit is

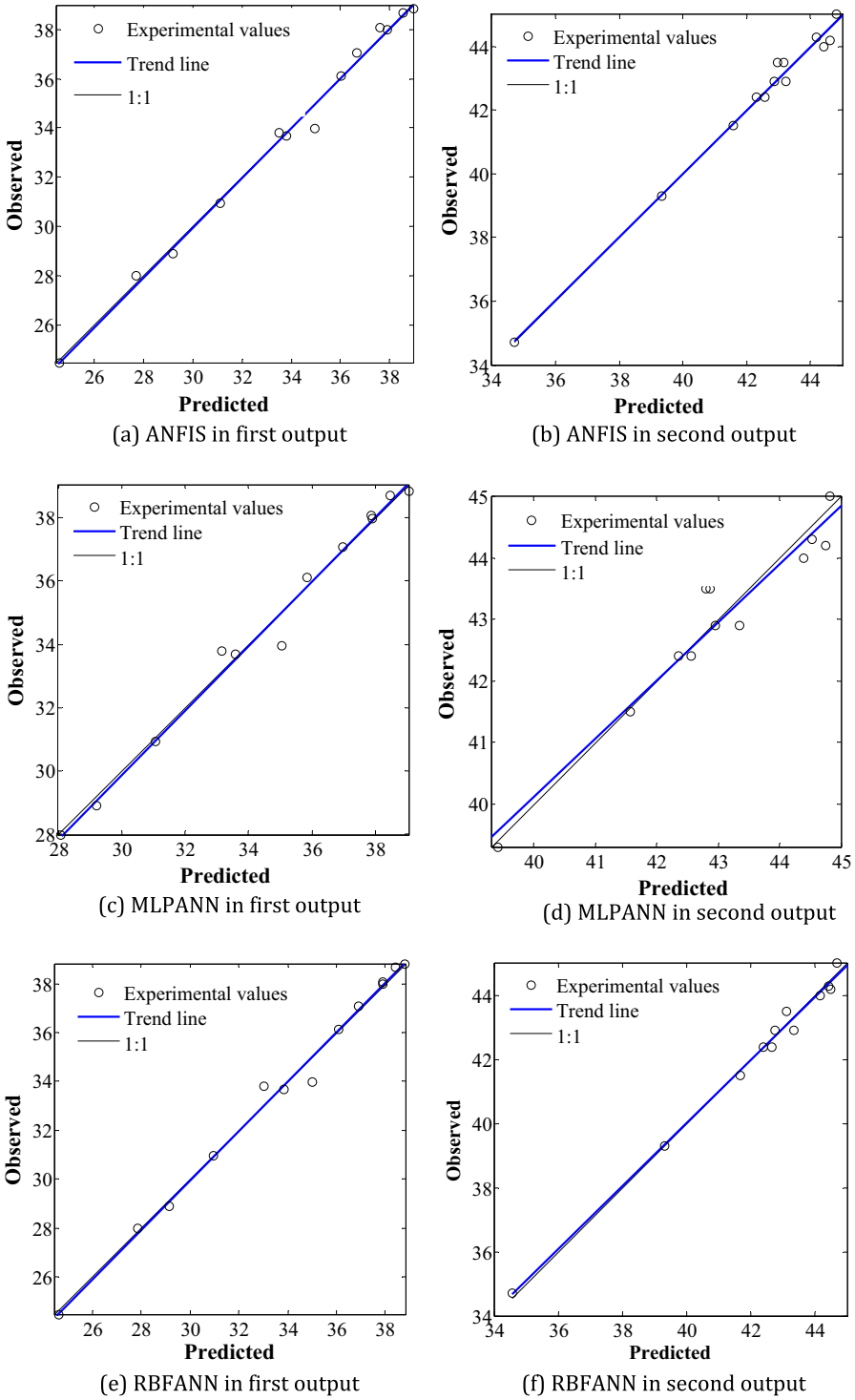

Fig. 6. Artificial neural network regression diagram for the first output (fluid outlet temperature) and for the second output (electrical efficiency).

equipped with a cupper sheet and tube collector and system. A view of the experimental setup is shown in Fig. 5(a–c). Because of having a closed circulation of working fluid in the thermal collector, in order to prepare the fluid for the next cycle of circulation, the working fluid must be cooled. This operation can be done by a heat exchanger. Working fluid have a closed flow circuit with a shell and tube heat exchanger with a counter flow designed to cool the working fluids after absorbing the heat in the collectors. Working fluid considered in the experiments is the zinc-oxide (ZnO)/water nanofluid. The ZnO nanoparticles, 100 nm in diameter, were dispersed in the water, with 0.2 wt.%, with an ultrasound mechanism and acetic acid (CH_3COOH) as surfactant. Fluid flow temperatures at the inlet and outlet of the heat exchanger and that of the collector are measured by K-type sensors that data are stored by a

Table 2
The performance of each model for two outputs.

Outputs	Methods	RMSE (%)	VAF (%)	MAPE	(R^2)
Fluid outlet temperature	MLPANN	0.3875	98.7644	0.7777	0.9879
	RBFANN	0.3911	99.2171	0.7481	0.9923
	ANFIS	0.3638	99.3222	0.8110	0.9934
Electrical efficiency	MLPANN	0.3621	93.3276	0.6330	0.9363
	RBFANN	0.2562	99.0387	0.5054	0.9906
	ANFIS	0.2675	98.9542	0.4882	0.9896

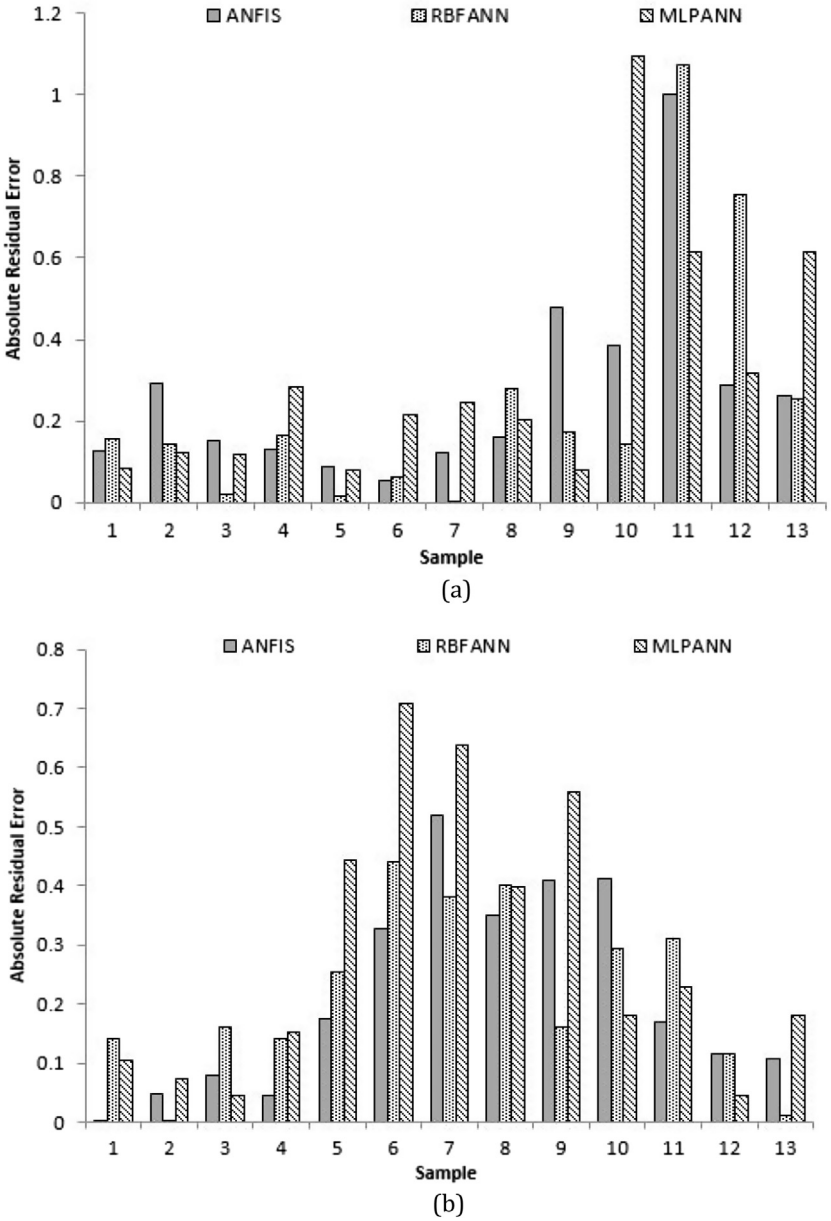

Fig. 7. Comparison absolute residual error between measurements and predicted results from three models for (a) fluid outlet temperature and (b) electrical efficiency.

Table 3
The p-values for comparing the accuracy (in terms of %RMSE) of all models.

		1st output (fluid outlet temperature)			2nd output (electrical efficiency)		
		MLPANN	RBFANN	ANFIS	MLPANN	RBFANN	ANFIS
P-value	MLPANN	*	<0.01+	<0.002−	*	<0.1+	<0.04+
	RBFANN	*	*	<0.001−	*	*	<0.0003+
	ANFIS	*	*	*	*	*	*

Plus/minus signs show that the method in each row have a better/worse performance that the method in corresponding columns.

k-type data logger; different points of photovoltaic (PV) surface temperature is measured by a portable K-type surface thermocouple. Digital multimeters are used to measure short-circuit and load currents, and open-circuit and load voltages. The total incident radiation is measured by a solar power meter (parallel to the photovoltaic surfaces). Working fluid mass flow rates are controlled and measured by a rotary flow meter. Experiments are performed at ten days with different weather condition. A set of the experiments consisted of thirteen data with different weather condition (solar radiation, ambient temperature, etc.) that recorded continuously each half an hour from 9:30 AM till 15:30 PM. More details of the experiments can be seen in previous work [1]. Experiments are repeated for ten days with different weather condition.

5. Results and discussion

In this work, the ability of the MLPANN, RBFANN and ANFIS for the prediction of fluid outlet temperature (first output) and electrical efficiency (second output) are examined. As it is mentioned before, these methods are constructed using three inputs and one output. Therefore, we have three methods for the first output and three methods for the second. The obtained results of the present paper are as follows:

(a) First, a cross-correlation between the observed and predicted values is obtained. As shown in Fig. 6, each of the six models has a high accuracy to predict the output. To have a better view about the models, the RMSE, the VAF, the MAPE and the R^2 values are also tabulated in Table 2. This table shows that despite the high ability of all models, the ANFIS for the first output and the RBFANN for the second output provides more reliable predication than the others.
(b) Next, Fig. 7 shows the absolute residual error between measures and the model output. The error bars displayed in this figure indicate that the deviation interval (0.053–0.999) of the predicted values from the ANFIS is smaller than that of the RBFANN (0.000787–1.07224) and MLPANNN (0.077–1.09483) for the first output (fluid outlet temperature). However, deviation interval of RBFANN (0.0019–0.44) to predict second output (electrical efficiency) is smaller than ANFIS (0.00219–0.52011) and MLPANN (0.0449–0.7079).

Moreover, one-way analysis of variance (ANOVA) and multiple comparisons were performed on three groups of predictions (two outputs) to compare the performance of the MLPANN, RBFANN and ANFIS. The %RMSE analysis statistically was verified significant for a p-value less than 0.05. The p-values for the three groups are shown in Table 3. In general, it was concluded that to predict the fluid outlet temperature, ANFIS provided lower %RMSE compared to those of the other two methods mentioned above. The reduction of the %RMSE in the ANFIS compared to that of the MLPANN ($p < 0.002$) and RBFANN ($p < 0.001$) was significant. Furthermore, for electrical efficiency, the RBFANN provides a significant reduction in the %RMSE ($p < 0.0003$) compared to that of the ANFIS. This, however, did not hold for prediction of electrical efficiency by MLPANN ($p < 0.1$).

6. Conclusion

In the recent years, the ANNs and fuzzy inference systems were employed for developing the predictive models to estimate the required parameters. In this study, the MLPANN, RBFANN and ANFIS were employed for modeling of a PVT/N system in various conditions. In general, the results showed that: (1) the MLPANN, RBFANN and ANFIS methods are capable of providing reasonably accurate estimations of outputs parameters, and (2) the input parameters (weather conditions) contain important information about modeling of the PVT. The accuracy of the MLPANN and RBFANN models was found to be similar in predicting electrical efficiency ($p < 0.1$). However, the RBFANN provided significantly lower %RMSE compared to that of the ANFIS ($p < 0.0003$). Moreover, the constructed ANFIS was found to result in a higher performance than the MLPANN ($p < 0.002$) and RBFANN ($p < 0.001$) in predicting fluid outlet temperature. Therefore, the results of this study reveal that the ANFIS, MLPANN and RBFANN are well suited for modeling nanofluids applications in solar systems.

The main focus of the paper is to find a simulation model for the PVT systems to help engineers to obtain an optimized design. Having a proper simulation modeling for the PVT systems, an optimized design can be obtained without any further experiments.

References

[1] M. Sardarabadi, M. Passandideh-Fard, S. Zeinali Heris, Experimental investigation of the effects of silica/water nanofluid on PV/T (photovoltaic thermal units), Energy 66 (2014) 264–272.
[2] S. Dubey, G.S. Sandha, G.N. Tiwari, Analytical expression for efficiency of PV/T hybrid air collector, Appl. Energy 86 (2009) 697–705.
[3] D. Atheaya, A. Tiwari, G.N. Tiwari, I.M. Al-Helal, Analytical characteristic equation for partially covered photovoltaic thermal (PVT) compound parabolic concentrator (CPC), Sol. Energy 111 (2015) 176–185.
[4] Minglu Qu, Jianbo Chen, Linjie Nie, Fengshu Li, Qian Yu, Tan Wang, Experimental study on the operating characteristics of a novel photovoltaic/thermal integrated dual-source heat pump water heating system, Appl. Therm. Eng. (2015), http://dx.doi.org/10.1016/j.applthermaleng.2015.10.126 (in press).
[5] J. Yazdanpanahi, F. Sarhaddi, M. Mahdavi-Adeli, Experimental investigation of exergy efficiency of a solar photovoltaic thermal (PVT) water collector based on exergy losses, Sol. Energy 118 (2015) 197–208.
[6] O. Rejeb, H. Dhaou, A. Jemni, A numerical investigation of a photovoltaic thermal (PV/T) collector, Renew. Energy 77 (2015) 43–50.
[7] C. Guo, J. Ji, W. Sun, J. Ma, W. He, Y. Wang, Numerical simulation and experimental validation of tri-functional photovoltaic/thermal solar collector, Energy 87 (2015) 470–480.
[8] M. Mohanraj, S. Jayaraj, C. Muraleedharan, Applications of artificial neural networks for refrigeration, air-conditioning and heat pump systems, a review, Renew. Sustain. Energy Rev. 16 (2012) 1340–1358.
[9] M.M. Papari, F. Yousefi, J. Moghadasi, H. Karimi, A. Campo, Modeling thermal conductivity augmentation of nanofluids using diffusion neural networks, Int. J. Therm. Sci. 50 (2011) 44–52.
[10] C. Renno, F. Petito, A. Gatto, Artificial neural network models for predicting the solar radiation as input of a concentrating photovoltaic system, Energy Convers. Manage. 106 (2015) 999–1012.
[11] A.N. Celik, Artificial neural network modelling and experimental verification of the operating current of mono-crystalline photovoltaic modules, Sol. Energy 85 (2011) 2507–2517.

[12] S. Leva, A. Dolara, F. Grimaccia, M. Mussetta, E. Ogliari, Analysis and validation of 24 h ahead neural network forecasting of photovoltaic output power, Math. Comput. Simul. (2015), http://dx.doi.org/10.1016/j.matcom.2015.05.010 (in press).
[13] A. Mellit, S. Sağlam, S.A. Kalogirou, Artificial neural network-based model for estimating the produced power of a photovoltaic module, Renew. Energy 60 (2013) 71–78.
[14] I. Ceylan, E. Gedik, O. Erkaymaz, A.E. Gürel, The artificial neural network model to estimate the photovoltaic module efficiency for all regions of the Turkey, Energy Build. 84 (2014) 258–267.
[15] M. Mohanraj, S. Jayaraj, C. Muraleedharan, Applications of artificial neural networks for thermal analysis of heat exchangers, a review, Int. J. Therm. Sci. 90 (2015) 150–172.
[16] N. Gunasekar, M. Mohanraj, V. Velmurugan, Artificial neural network modeling of a photovoltaic-thermal evaporator of solar assisted heat pumps, Energy 93 (2015) 908–922.
[17] H. Kurt, M. Kayfeci, Prediction of thermal conductivity of ethylene glycol–water solutions by using artificial neural networks, Appl. Energy 86 (2009) 2244–2248.
[18] M. Hojjat, S.G. Etemad, R. Bagheri, J. Thibault, Thermal conductivity of non-Newtonian nanofluids: experimental data and modeling using neural network, Int. J. Heat Mass Transf. 54 (2011) 1017–1023.
[19] S. Atashrouz, G. Pazuki, Y. Alimoradi, Estimation of the viscosity of nine nanofluids using a hybrid GMDH-type neural network system, Fluid Phase Equilib. 372 (2014) 43–48.
[20] F. Yousefi, H. Karimi, M.M. Papari, Modeling viscosity of nanofluids using diffusional neural networks, J. Mol. Liq. 175 (2012) 85–90.
[21] H. Karimi, F. Yousefi, Application of artificial neural network–genetic algorithm (ANN–GA) to correlation of density in nanofluids, Fluid Phase Equilib. 336 (2012) 79–83.
[22] A.K. Santra, N. Chakraborty, S. Sen, Prediction of heat transfer due to presence of copper–water nanofluid using resilient-propagation neural network, Int. J. Therm. Sci. 48 (2009) 1311–1318.
[23] B. Vaferi, F. Samimi, E. Pakgohar, D. Mowla, Artificial neural network approach for prediction of thermal behavior of nanofluids flowing through circular tubes, Powder Technol. 267 (2014) 1–10.
[24] S.A. Kalogirou, Applications of artificial neural networks for energy systems, Appl. Energy 67 (2000) 17–35.
[25] J. Kennedy, R. Eberhart, Particle swarm optimization, in: Conf. Neural Networks, 1995, pp. 1942–1948.
[26] X. Hu, R. Eberhart, Adaptive particle swarm optimization: detection and response to dynamic system, in: Congress on Evolutionary Computation (CEC), 2002, pp. 1666–1670.
[27] X. Li, K.H. Dam, Comparing particle swarms for tracking extrema in dynamic environments, in: Congress on Evolutionary Computation (CEC), 2003, pp. 1772–1779.
[28] A. Carlisle, G. Dozier, Adapting particle swarm optimization to dynamic environment, in: Proceeding of the International Conference on Artificial Intelligence, 2000, pp. 429–434.
[29] M. Seyedmahmoudian, S. Mekhilef, R. Rahmani, Y. Rubiyah, A. Shojaei, Maximum power point tracking of partial shaded photovoltaic array using an evolutionary algorithm: a particle swarm optimization technique, J. Renew. Sustain. Energy 6 (2) (2014) 023102, http://dx.doi.org/10.1063/1.4868025, ISSN 1941-7012.